Full scale experiments to examine the role of deadwood on rockfall dynamics in forests

Adrian Ringenbach[1,2,4], Elia Stihl[1,2], Yves Bühler[1,2], Peter Bebi[1,2], Perry Bartelt[1,2], Andreas Rigling[3,4], Marc Christen[1,2], Guang Lu[1], Andreas Stoffel[1,2], Martin Kistler[1], Sandro Degonda[1], Kevin Simmler[1], Daniel Mader[3], and Andrin Caviezel[1,2]

[1]Climate Change, Extremes, and Natural Hazards in Alpine Regions Research Center CERC, 7260 Davos Dorf, Switzerland
[2]WSL Institute for Snow and Avalanche Research SLF, 7260 Davos Dorf, Switzerland
[3]Swiss Federal Institute for Forest, Snow and Landscape Research WSL, Zürcherstrasse 111 8903 Birmensdorf, Switzerland
[4]Department of Environmental Systems Science, Institute of Terrestrial Ecosystems, ETH Zürich, Zurich, Switzerland

Correspondence: Adrian Ringenbach (adrian.ringenbach@slf.ch)

Abstract. Forests are rockfall-protective ecological infrastructures, as a significant amount of kinetic energy is absorbed during consecutive rock-tree impacts. Although many recent works have considered rock impacts with standing trees, the effect of lying deadwood in forests has not yet been considered thoroughly, either experimentally or numerically. Here, we present a complete examination of induced rockfall experiments with sensor-equipped, 45 kg, artificial rocks on a forested area in three different management stages. The trilogy is conducted in a spruce forest stand (i) in its original state of forest, (ii) after a logging operation with fresh, lying deadwood and (iii) after the removal of the deadwood. The tests allow us to directly quantify the effect of fresh deadwood on overall rockfall risk for the same forest (slope, species) under three different conditions. The study yields quantitative results on the barrier efficiency of the deadwood logs as only 3.6 % of the rocks surpass the deadwood section. The mean run-out distance is reduced by 42 %. Conversely, the run-out distance increases by 17 % when the cleared stand is compared to the original forest. These results quantitatively confirm the benefits of nature-based mitigation measures integrated into forestry practice, whose detailed effect has to be scrutinized for higher rockfall energies. Based on the experimental results, we extended a modern rockfall code by three-dimensional deadwood logs, to incorporate such complex, but realistic forest boundary conditions.

1 Introduction

Rockfall is a common natural hazard in mountain regions. Up to certain rockfall magnitudes, protection forests are effective ecological infrastructures to reduce rockfall intensities and thus the damage on vulnerable facilities as falling rocks are decelerated by consecutive tree impacts. This has been shown by real scale experiments at the slope scale in a mixed Abies-Picea-Fagus forest (Dorren and Berger, 2005) as well as on single trees of different species including *Picea abies*, (Lundström et al., 2009) and *Ailanthus altissima*, (Wunder et al., 2018). Implementation of these findings into three-dimensional rockfall models, e.g. Rammer et al. (2010); Dorren (2012); Toe et al. (2017); Lu et al. (2020), facilitated additional investigations to

quantify the protective capacity of mountain forests using numerical tools at the forest stand (Stoffel et al., 2006; Woltjer et al., 2008; Moos et al., 2017) and regional scales (Dupire et al., 2016; Lanfranconi et al., 2020).

Experimental tests to investigate the role of deadwood for rockfall mitigation have also been performed at the laboratory (Ammann, 2006; Olmedo et al., 2015) and slope (Bourrier et al., 2012) scales. The laboratory studies provided the first quantitative insights into the protective effects of deadwood but do not accurately represent natural deadwood configurations after disturbances since the investigators used clumped *Picea abies* and *Fagus sylvatica* specimens with relatively small mean diameters of 26 cm and 6 cm (Ammann, 2006; Olmedo et al., 2015). The field studies of Bourrier et al. (2012) used larger 63 cm diameter logs fixed to tree stumps using steel cables. How deadwood is naturally fixed (jammed) between trees and the ground is essential to understand its protective capacity and therefore man-made fixations may also not represent natural conditions in mountain forests. As a consequence, present approaches to include deadwood into a three-dimensional rockfall model are based on slope or roughness adaption methods combined with higher, and empirically determined, rock-ground restitution coefficients (Fuhr et al., 2015; Costa et al., 2021).

Neither the different experimental nor the modeling approaches take piled stems into account, which are often the result of uprooted trees during windthrow events. Beside windthrows (Feser et al., 2015), also bark beetle outbreaks (Jönsson et al., 2009) and forest fires (Mozny et al., 2021; Jain et al., 2020) are likely to increase in frequency or amplitude due to climate change and land-use legacies. Allowing natural processes without salvage logging after windthrow and without sanitary felling after bark beetle are increasingly promoted as adequate management option (Kulakowski et al., 2017; Sommerfeld et al., 2021). In rockfall protection forests, it is decisive to know more on the short- and long-term effects of piled stems on rockfalls after natural disturbances or management interventions.

In this paper, we present the results of three induced rockfall experiments within the same mountain forest but in three different management states. First, we performed rockfall experiments in the original, undisturbed forest. In the next series of tests, the effect of lying, partly piled, fresh deadwood in the upper third of the slope was tested. The "deadwood" was created after a forest management intervention and was therefore in a fresh condition with maximal physical resistance. In the final test series, the deadwood was cleared (the final forest was, therefore, sparser than the original forest). All three tests were performed in the same spruce stand to explore the protective effect of lying deadwood quantitatively. We extended a three-dimensional rockfall code with truncated cones acting as deadwood logs to imitate the experimental setting numerically. An in-depth model calibration was performed based on the experimental results. As nature-based mitigation measures are expected to gain in importance, an accurate treatment thereof in numerical tools is essential for future hazard assessment procedures.

2 Material and methods

2.1 Study site: Surava

The study site (46.65720° N, 9.60497° E, 1120 m a.s.l.) covers 0.54 ha of north-west exposed, roughly 35° steep mountain forest in the community Surava within the municipal area of Albula/Alvra, Switzerland. In a complete forest inventory the diameters at breast height (DBH), tree species and GNSS-positions of all trees with DBH $\geq$ 8 cm were recorded, resulting

in a total of 462 trees, a stand density of 855 trees ha^{-1} and a mean DBH of 23.9 $\pm$ 11.7 cm, see Figure 1.a). The principal tree species are Norway spruce (78.8 %, *Picea abies* (L.) Karst.), European larch (9.5 %, *Larix decidua* Mill.), mountain pine (6.7%, *Pinus mugo* subsp. uncinata (DC.) Domin.) and silver fir (4.1 %, *Abies alba* Mill.). Further single rowans (*Sorbus aucuparia* L.), beeches (*Fagus sylvatica* L.) and whitebeams (*Sorbus aria* (L.) Crantz) were registered.

2.2 Experimental set-up

Rockfall experiments were conducted during three different states of forest: in the original forest (**ORG**), after a logging operation, but before the removal of the lying, partly piled deadwood (**DW**), and subsequently with this area cleared (**CLR**). The intention of the logging operation was the creation of a regeneration gap, a small-sized clear-cut, in the upper part of the even-aged spruce forest. Its area covered about 700 m^2 and comprised 53 trees, of which 26 trunks were left lying for the CLR-experiments (Fig. 1.a). We used perfectly symmetrical reinforced *EOTA* concrete rocks (ETAG 027, 2013) with a mass of 45 kg and a diameter of 0.29 m (Fig. 3.d). The diameter of a *EOTA* rock is defined as the distance between two opposing flat surfaces. This mass allowed still a manual rock handling, even if rocks stuck between deadwood logs. In a borehole through its center of mass, in situ StoneNode v1.3 sensors were mounted to record rotational velocities (ω) in all three axis up to 69.8 rad·s^{-1} (= 4000°·s^{-1}) and accelerations up to 3922.66 m·s^{-2} (= 400 g) with a sampling rate of 1 kHz (Niklaus et al., 2017; Caviezel et al., 2018).

The rocks were repeatedly released manually from the same starting position at 1118.5 m a.s.l.: 42 runs in the **ORG**, 28 runs in the **DW**, and 41 runs in the **CLR** state of the forest, of which at least 73 % per state include the in situ sensor streams. The deposition points of the rocks were measured with a high-precision Trimble GeoXH differential handheld GNSS reduced to a mean horizontal accuracy of 1.6 m in this steep, north-west-facing, forested slope. The rocks were winched back from their deposition point to the forest road and from there transported by four-wheel motorcycle back to the release point.

To compare the deposition pattern between the three states of the forest quantitatively, the geographic mean centre (GMC), the third standard deviation ellipse (SDE) and its radius of the long (SDE$_{la}$) and short axis (SDE$_{sa}$) were calculated based on the python code provided by Schelp (2018). The mean run-out distance (MROD) is the euclidean, slope parallel distance between the release point and GMC.

2.3 Sensor data processing

In order to detect frontal impacts (FI) on opposing objects such as standing trees, overturned root plates or larger rocks, we applied gyroscopic data analysis, rather than evaluating the acceleration data, since the latter varies strongly depending on the incoming translation velocity and especially the material being hit. Regardless of the material, after an FI, a sharp reduction in the resulting rotational velocity will occur. We generated smoothed gyroscopic data streams by applying five different moving window sizes (0.001 s, 0.021 s, 0.061 s, 0.101 s, and 0.151 s, Fig. 3.e) to reliably detect such abrupt changes in the resultant gyroscopic data stream. On each of these streams, we executed the *Matlab* function *ischange* (Killick et al., 2012) with its $linear$ method. The corresponding, empirically determined segment slope thresholds (≤ -100, ≤ -29, ≤ -21, ≤ -9.75, and

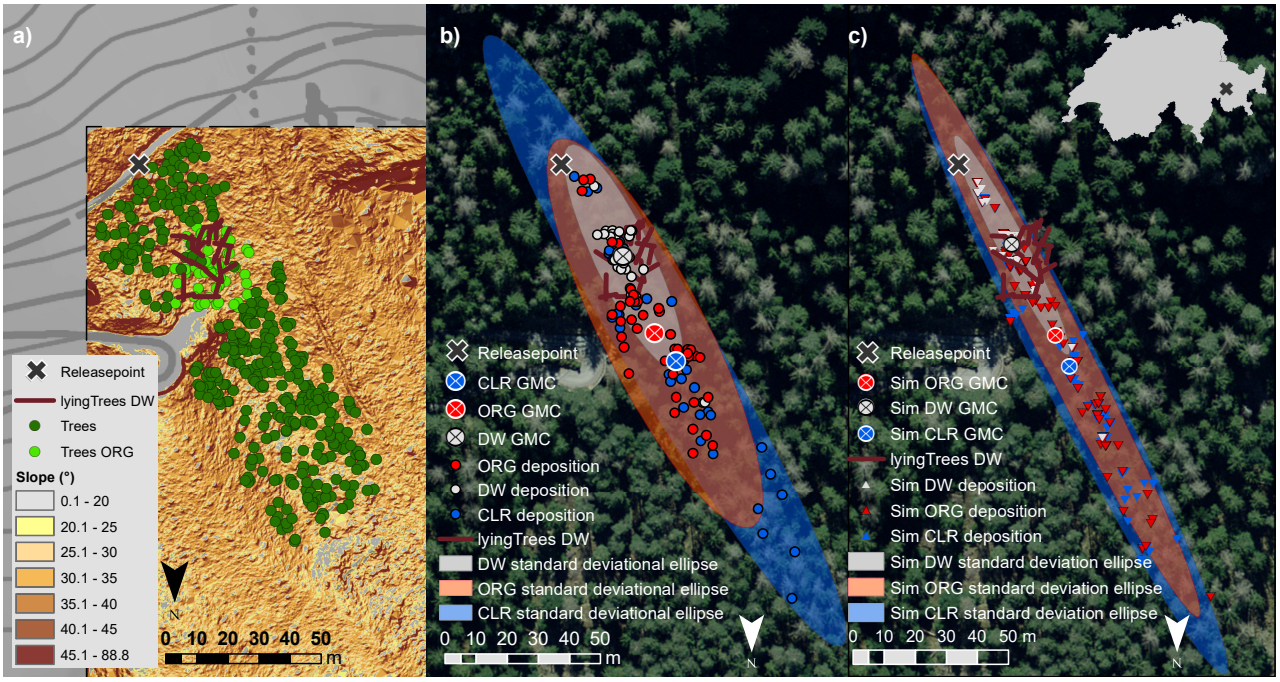

Figure 1. Overview of the experimental test site Surava: a) Slope map with the standing trees during the whole trilogy (dark green circles), during ORG state (light green circles) and lying deadwood during DW (brown lines). b) Deposition points of all 111 runs of the 45 kg $EOTA_{111}$ rocks including all three states of the forest: ORG in red, fresh DW in grey and CLR in blue. The corresponding geographic mean centers (GMC) are shown with crossed symbols in the corresponding color. Additionally, the third standard deviation ellipse (SDE) of each data set, are depicted as transparent ellipses. c) deposition point of the total 300 simulated trajectories under consideration of the three states of the forest. The GMC and SDE are in the corresponding colors of the experimental results. Source of topographical map (a) and orthophoto (b,c): Federal Office of Topography

≤ -6.5) define the minimal decrease of rotational velocity within each moving window to flag a FI (Fig. 3.f). A minimum of three thresholds must be reached to flag a FI.

2.4 Rockfall simulations

The experimental rockfall trilogy was emulated with a rigid body rockfall code that includes compactable soils (Lu et al., 2019) and standing single trees (Lu et al., 2020). The used tree height in RAMMS::ROCKFALL was estimated based on $H = DBH^{\frac{1}{1.25}}$ (e.g. Dorren (2017)). To represent the conditions of the **DW** state of the forest, we introduce three-dimensional, rigid, truncated cones. During fieldwork, all 26 trunk GNSS positions were recorded. Still missing were the exact diameters and the height above the ground of every log end, required as input parameters for the generation of the individual deadwood cone in RAMMS::ROCKFALL. As a realistic but simplified approach, we assumed a uniform maximal diameter of 40 cm for all

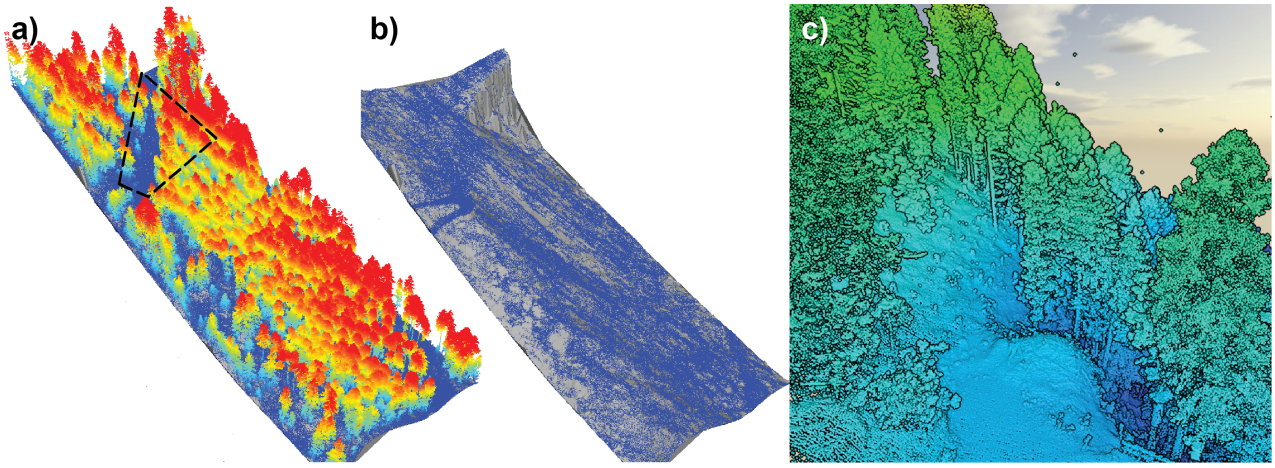

Figure 2. a) The acquired LiDAR point cloud colored according to the height above ground (blue = 0 m, red $\geq$ 23 m). b) LAStool post-processed ground points used to generate a high-resolution digital surface model for the rockfall simulations. c) Zoomed-in section of the cleared area as indicated in a). The mesoscale surface roughness is clearly discernible in the ground points in the cleared area as well below the remaining tree canopy.

deadwood-logs. If logs were lying on top of each other, we considered the chronologically first recorded log in the GNSS-file as the lower log with ground contact, and the latter ones piling up on top of it.

Current surface models from the Swiss Federal Office of Topography swisstopo are available with resolutions as fine as 0.5 m grid size. The need to account for mesoscale roughness effects as well as customized ground point detection algorithms nonetheless demanded a site-specific airborne LiDAR mission. The LiDAR point cloud has a density $\geq$ 500 points$\cdot\mathrm{m}^{-2}$ and was scanned by a Trimble AC60 sensor, after the CLR experiments (Fig. 2). The generated digital surface models with a resolution of 0.05 m, processed in the LAStool-framework with the $-extrafine$ option, specialized to detect ground points in steep mountainous regions (Isenburg, 2021), were used for the simulation of all states of the forest.

The soil mechanical strength M_E and the scar drag coefficient C_d are the soil parameters to calibrate (Lu et al., 2019; Caviezel et al., 2019b). We performed simulations sweeps within the relatively wide range of $0.8 \leq M_E \leq 2.6$ kN $\cdot\,\mathrm{m}^{-2}$ and $1.7 \leq C_d \leq 3.0$ where the parameters of soft soils should be located. Runs with 300 orientations were performed to narrow down the parameter ranges for the in-depth calibration. Subsequently a model run with 3000 initial rock orientations per forest state and M_E and C_d pairs within the ranges of $1.6 \leq M_E \leq 2.1$ kN $\cdot\,\mathrm{m}^{-2}$ and $2.6 \leq C_d \leq 3.1$ and with a step size of 0.1 was performed. The calibration is based on the comparison of simulated versus experimental deposition patterns, more precisely its standard deviational (or directional distribution) ellipse. The fit per state was calculated and summed up in the overall fit (OF_{3000}) over all states:

$$S_{\mathrm{FIT}} = |\mathrm{MROD} - \mathrm{MROD}_{sim}| + |\mathrm{SDE_{la}} - \mathrm{SDE_{lasim}}| + |\mathrm{SDE_{sa}} - \mathrm{SDE_{sasim}}| \quad (1)$$

where the scenario S is either **ORG**, **DW**, or **CLR**. The sum of all the scenario fits amount to the overall fit

$$\mathrm{OF}_{3000} = \mathrm{ORG}_{\mathrm{FIT}} + \mathrm{DW}_{\mathrm{FIT}} + \mathrm{CLR}_{\mathrm{FIT}} \tag{2}$$

This metric allows to quantify the differences between experimental scenarios as well as the congruence between experiment and simulation. To reduce scaling effects due to the massively higher number of simulations (3000) relative to the experiments, additionally packages of 100 trajectories were randomly drawn and compared to the results of the experiments, consequently labeled as OF_{100} .

3 Results

3.1 Rockfall experiments

None of the 111 released EOTA_{111} rocks were capable of breaking a tree or a deadwood log. The effect of lying deadwood had an important influence on the observed rockfall dynamics for the investigated weight class summarized in Tab. 1 and visualized in Fig. 1.b: The mean slope parallel run-out distance (MROD) is reduced by 42.1% when comparing the **DW** to the **ORG** state of the forest. The effect of the removed standing trees between **ORG** and **CLR** is visible in the prolongation of the MROD by 17.7%. The $\mathrm{DW}_{\mathrm{MROD}}$ reduction is accompanied by an increase of the mean shadow angle DW_{α} by 1.3° and 1.4° compared to ORG_{α} and CLR_{α}. The use of standard deviation analysis implies an compliant data set. The presented data confirms this assumption, except for the longitudinal deposition pattern for the **DW** state, based on the normal-distribution test ($scipy.stats.normaltest$, α = 0.05) for the x- an y- deposition coordinates, after a conducted principal components rotation ($sklearn.decomposition.PCA$).

The similar grouping among the forest configurations is also for the in situ measured data visible: The two-sample t-test produced significant (α = 0.05) differences between the mean run time, the maximal accelerations of the **DW** state and the corresponding variables of the **ORG** and **CLR** states. Within **ORG** and **CLR**, the differences are not significant within the chosen level.

The number of detected FI on opposing objects was between 0.90 (**ORG**) and 0.43 (**DW**) per run. Based on the slope parallel distance between starting and deposition point and the run time from the sensor stream, the mean velocity for each run is calculated. The longer MROD influences also the mean run time, but not linearly: rocks in the **DW** state were moving on average for 14 s, which results in a mean velocity of 2.9 m s^{-1}. The states **ORG** and **CLR** feature run times of 19 s and 23 s, respectively. In conjunction with their longer run-out distances, **ORG** and **CLR** surpass the **DW** state by a 28% higher velocity.

3.2 Rockfall Simulations

The parameter pair $M_E = 2.0$ and $C_d = 2.9$ yield the best overall fit (OF) over all 3000 simulation ($\mathrm{OF}_{3000} = 83.0$ m) and of any randomly sampled package of 100 trajectories ($\mathrm{OF}_{100} = 58.7$ m). The parameter robustness is highlighted by the 10^{th} best fit: $\mathrm{OF}_{3000}^{\mathrm{R10}} = 86.5$ m only having a 4.3 % higher deviation. The following analysis (Tab. 1 and Fig. 4) focuses on the

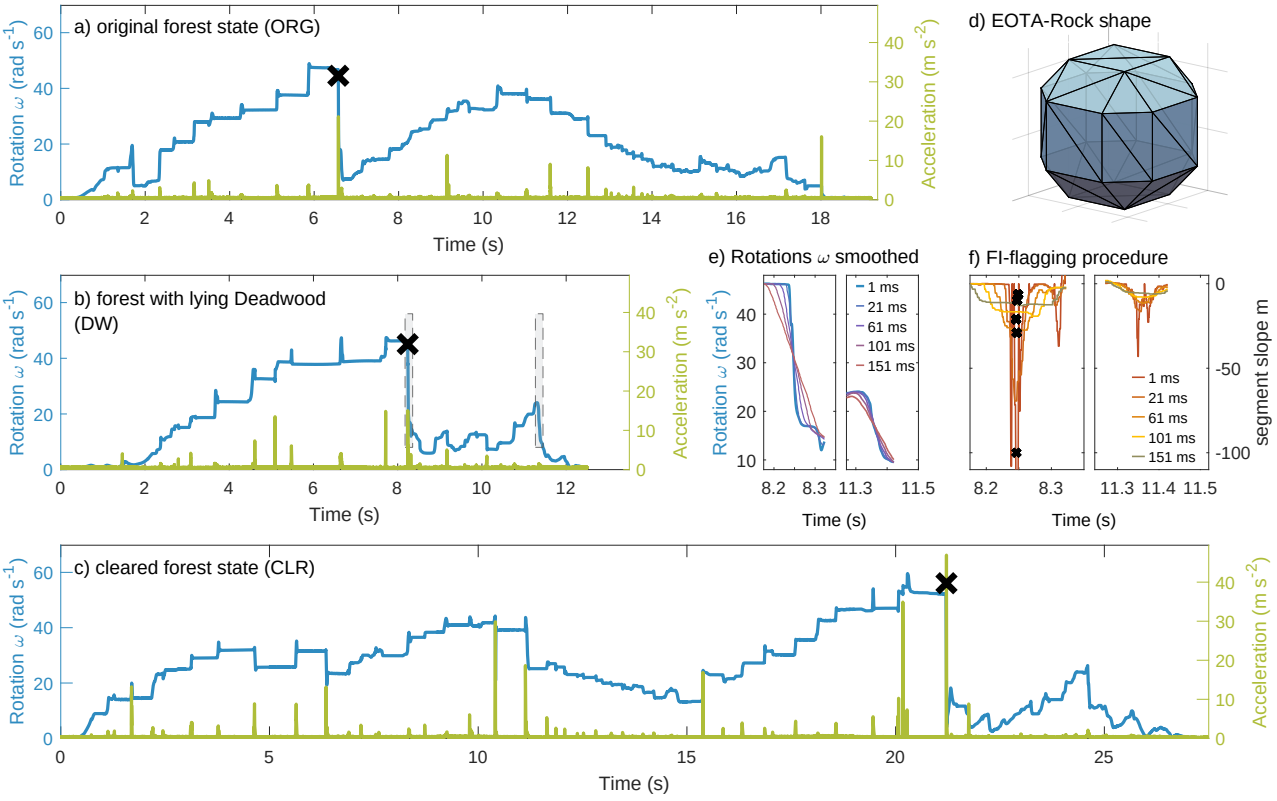

Figure 3. Example of three typical StoneNode data streams a)-c) measured within the 45 kg EOTA_{111} rocks (d): in blue the resulting rotational velocities, in green the resulting impact accelerations of a) an ORG-run, b) a DW-run and c) a run within the CLR-stand. The confirmed frontal impacts (FI) therein are marked as large black crosses, their flagging procedure exemplified in e) and f) for two hits outlined in gray in c). (e) Smoothed rotations ω with different moving window sizes and (f) segment slopes m of linear segments in smoothed ω. If falling below the moving-window specific threshold, the impact is flagged as possible FI (small black crosses), prevailing as confirmed FI if at least three flags are produced for the same impact.

trajectory-package with the best OF_{100}. The experimentally observed MROD reduction of the deadwood was recognizable in the simulations: The **DW**-simulations had a slightly (5.9 m, 14%) shorter MROD as the experiments, but a similar length of the $\mathrm{SDE}_{\mathrm{la}}$. While the MROD and its $\mathrm{SDE}_{\mathrm{la}}$ of the **CLR** state-simulations were both within the experimental GNSS-accuracy, the ORG simulations show a good fit in the MROD, but a larger longitudinal spread of $\mathrm{SDE}_{\mathrm{la}}$ as recorded during the experiments. The overall good fit of the simulated MROD consequently leads to a good agreement of the simulated mean shadow angles. The simulated mean run time for the shorter runs of the **DW** state are consistent with the experiments (-4.4%). The run times for the **ORG** (+45.8%) and **CLR** (+37.6%) are by contrast considerably overestimated and the velocities therefore underestimated.

Although the trend of the simulated average maximum accelerations between the states of the forest is correct, the simulations globally underestimate the experimental values by roughly 40%. The simulated maximal rotational velocities per run are

Table 1. Resulting statistics of the experiments (left) and Simulations (right) for the original state of the forest (**ORG**), the state with lying, fresh deadwood (**DW**) and the deadwood cleared area (**CLR**)).

		Experiments			Simulations		
		ORG	**DW**	**CLR**	**ORG**	**DW**	**CLR**
N° Runs/with Sensor data		42/42	28/21	41/34	100/100	100/100	100/100
mean run-out distance± SD	(m)	74.3±27.2	43.1±15.4	87.5±42.7	75.4±39.8	37.2±15.7	88.4±43.4
mean shadow angle± SD	(°)	34.4±1.2	35.6±0.8	34.2±1.3	34.9±1.3	36.2±0.8	34.6±1.7
mean run time ± SD	(s)	19.2±6.4	13.7±5.2	21.2±11.4	27.7±16.2	13.1±6.0	31.5±16.6
mean max. acc. per run ± SD	(g)	265.8±98.1	217.0±83.0	265.3±85.4	152.6±49.4	138.5±47.2	164.3±45.7
mean max. ω per run ± SD	($rad \cdot s^{-1}$)	48.3±6.5	45.6±6.3	45.7±10.5	30.7±3.6	30.7±3.7	31.1±3.1
mean average ω per run ± SD	($rad \cdot s^{-1}$)	20.8±3.3	17.3±2.8	18.7±4.5	14.2±2.0	14.6±2.2	14.4±2.0
mean N° *FI* per run ± SD	(-)	0.88±0.89	0.43±0.51	0.57±0.65	-	-	-
mean N° *FI* per run time ± SD	(s^{-1})	0.049±0.049	0.032±0.041	0.031±0.043	-	-	-
mean velocity ± SD	(ms^{-1})	3.7±1.2	2.9±0.6	3.7±0.8	3.0±0.4	3.1±0.5	3.0±0.4

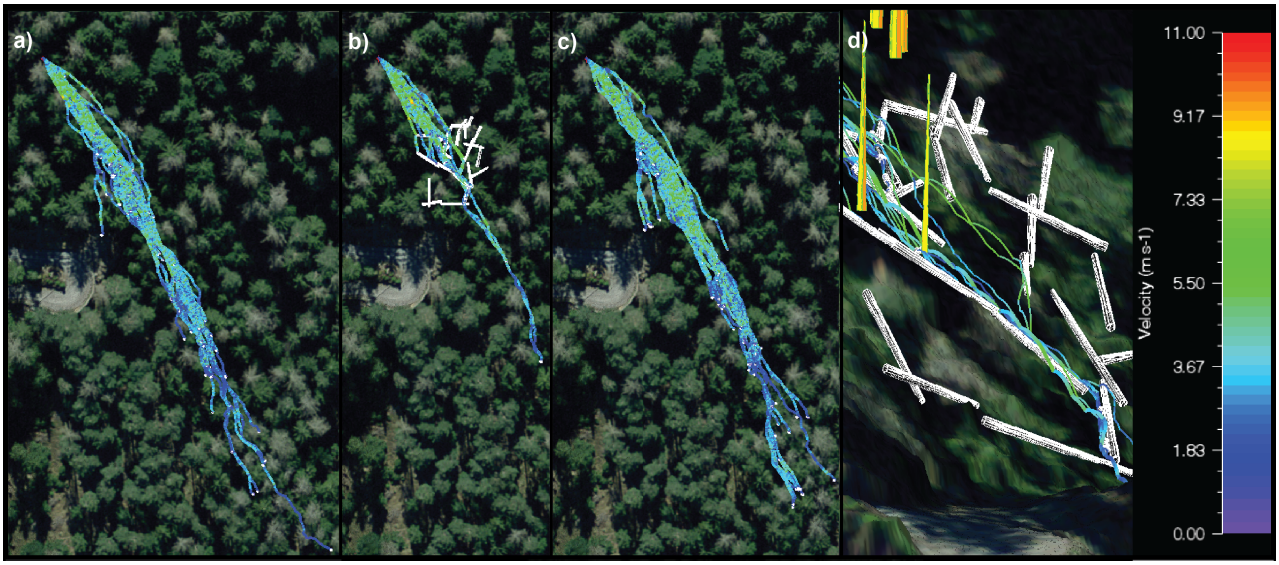

Figure 4. Velocity comparison of the 100 simulated rockfall trajectories in the a) ORG, b) DW and c) CLR states of the forest. d) Detailed three-dimensional view from above the forest road of the trajectories in b) within the deadwood section: lying deadwood in white, standing trees in yellow. Source of orthophoto (a - d): Federal Office of Topography

between 31.9 % - 36.4 % lower as the results of the experiments. A less pronounced underestimation, 15.6% for **DW**, 30% for **ORG**, was detected for the mean rotational velocities. Within the simulated rotational data stream, no FI could have been detected with the same thresholds.

4 Discussion

The important effect of lying deadwood on the rockfall dynamics of 45 kg rocks is demonstrated by the presented experimental results. Although a certain rockfall protection effect by deadwood was known in practice, it has never been investigated with such a systematic, full-scale experiment. One out of 28 released rocks (3.6%) surpassed the piled deadwood section in the upper third of the experimental **DW** slope. Compared to **ORG** and **CLR** where 81.0% and 78.1% of the rocks passed the deadwood area, the deadwood stopping capacity due to the deadwood barrier effect within this shape class is substantial. Even if the GNSS-uncertainty is taken into account still 71.4% and 73.2% of the released rocks within the **ORG** and **CLR** set-ups reached the forest below the deadwood section. This is the main difference from the findings of Bourrier et al. (2012), where the vast majority of the released rocks impacted the four felled deadwood trunks (85.7%), but only 8.5% of the rocks stopped immediately. The differences in experimental design and results underline the assumption, that realistic deadwood configurations have a better protective function than deadwood with direct ground contact. The ratio between a rock and deadwood log diameter might play an important role, both in terms of hindering rolling over of the obstacle as well as in terms of breaking prevention, as the reported ratio in Bourrier et al. (2012) < 1 and the here observed ratio > 1 imply. If the protective effect of deadwood is deliberately used as a silvicultural measure, we recommend arranging logs on top of each other behind tree stumps (as discussed by Olmedo (2015); Olmedo et al. (2020)) to achieve a more favourable rock-to-deadwood diameter-ratio. Similar to the mean slope of Bourrier et al. (2012), the presented study site features an acceleration zone of roughly 37° but regrades in the deadwood area to 33°. This flattening might additionally explain the higher stopping capacity of the deadwood in this study.

Although run-out estimations with the shadow angle method have lost importance, since three-dimensional rockfall simulations prevail, it is shown that this parameter is increased by the deadwood. As the amount of the absolute angle increase is strongly dependent on the location of the deadwood section, which was in this study in the upper third, a general shadow-angle-reduction due to deadwood is not applicable.

According to the measured in situ data (Tab. 1), the states of the forest **ORG** and **CLR** with high maximal accelerations per run also showed higher mean velocities than **DW**. These measurements underlie the assumption that higher velocities increase the probability of harder impacts. Additionally, longer MROD and run times resulted in a higher probability of hitting hard ground material, especially when rocky sections are not randomly distributed across the study site and more frequent at the lowest part of the slope. This effect was not visible within the simulations, as for the whole area, one single ground parameter-set was used. This additionally explains why velocities of short trajectories (**DW**) are modeled more precisely as the velocities of trajectories with longer MROD (**ORG** and **CLR**). Locally higher M_e and lower C_d values could solve this issue. However, since the calibrated data should serve to model rockfall in similar forests, it is not debatable to include details down to the single rock scale.

The detected maximal rotational velocities per run are slightly higher within this campaign, as expected from the empirically derived mass - mean rotational velocity relationship from open-field experiments (Caviezel et al., 2021). However, experimental and simulated results for rotational velocities differ substantially. While the standard deviations of the mean rotational velocities

between the experiments and the simulations overlap at least for two (**DW** and **CLR**) of the three forest states, no overlap is given for the maximal rotational velocities per run. Nevertheless, these maximal rotational velocities show a distinctly higher standard deviation than the simulated and the mean values. This might corroborate the considerable influence of local disparities in soil and tree conditions, leading to a higher acting torque-variability on the rocks, resulting in higher maximal rotational velocities.

The **DW** sensor streams feature less FI per run than the other two states. As most of the rocks stopped within the deadwood section, a higher ratio of impacts was expected. Surprisingly, the mean number of frontal impact per run lies well below 50 %. Hence, the stopping process in the deadwood section is not abrupt enough to classify as frontal impact like the hit of a standing tree. Additional clarification can be offered, if the FIs are evaluated as frontal impacts per runtime ($\mathrm{FI} \cdot \mathrm{s}^{-1}$). (Tab. 1): Even if the **ORG** state still has the highest $\mathrm{FI} \cdot \mathrm{s}^{-1}$, the **CLR** state shows slightly lower values than the **DW** state. The shortest mean runtime implies the smallest possibility to experience a FI in the deadwood state. This is not outweighed by the stopping process within the deadwood, in particular because it apparently features a more complex, temporally stretched, behavior. Although without visual verification not all questions concerning the influence of rotational velocities on FI can be solved, Figure 3.b) illustrates, that solely acceleration data would perform worse: Of the three impacts with $\geq 10\ \mathrm{m} \cdot \mathrm{s}^{-2}$, the first two impacts entail increasing rotational velocities, which seems unlikely for FI on an opposing object. The third impact, however, is related to a severe drop of the rotational velocity. Compared with the overall measured accelerations of the **CLR** state (Fig. 3.c), the **DW**-impacts (Fig. 3.b) are much softer, but comparable with the impacts of **CLR** in the corresponding time range, and thus slope area. This consolidates the assumption that acceleration data feature dependencies regarding the soil characteristics and hence the used FI detection-method based on gyroscopic data is more reliable. The FI of the depicted sensor streams in Figure 3 shows a reduction by more than 50 % from > 40 rad ($> 2000° \cdot \mathrm{s}^{-1}$) to <20 rad ($< 1000° \cdot \mathrm{s}^{-1}$), while the corresponding accelerations differ with values ranging from 15.0 $\mathrm{m} \cdot \mathrm{s}^{-2}$ to 46.9 $\mathrm{m} \cdot \mathrm{s}^{-2}$ by more than 300 %. The FI detection within the simulations was not possible based on the same thresholds, due to the used and recommended standard computational output time-step of 0.02, which is too low compared to the 1 kHz sampling rate of the StoneNode sensors.

The protective effect of lying deadwood can only be emulated by rockfall simulations if deadwood configurations can be added realistically into the code. Here, all three states of the forest, incorporating the exact GNSS position as three-dimensional cones for standing and lying trees alike could be reconstructed as input scenarios for the rockfall simulations. This strict adherence to realistic site conditions enhances the significance of the model output for hazard assessment significantly. The inclusion of the deadwood logs as three-dimensional cones resulted in simulations with a realistic deposition pattern. Apart from the depicted barrier effect of single, near-slope deadwood logs, piled trunks after wind-throw events can now be incorporated into simulations. Additionally, a tunnel effect can be modeled: rocks can slip under deadwood, which is essential or if the deadwood branches are still fresh and support the log above ground. In such cases, other methods like adapting the slope in the corresponding grid cells, overestimate the deadwood effect and experience drawbacks (Fuhr et al., 2015; Costa et al., 2021).

Nevertheless, the simulations do not feature the observed experimental lateral spread. A possible explanation lies in the post-experimental timing of the LiDAR flight: the deadwood clearing work may have changed the local topography slightly,

which was during the **ORG** and **DW** experiments partially responsible for the lateral spread, since the $\mathrm{CLR_{FIT}}$ generally fits best for all soil parameters-sets.

One possible explanation of the overestimated mean runtimes in the simulations (Tab. 1) could be caused by a critical issue with any numeric rockfall code: an accurate stopping criterion. This criterion describes the minimal total kinetic energy of the rock below which the simulation is terminated. To examine the contribution to this overestimation, we calculated the mean velocity on the last 2 m of travelling distance ($\mathrm{ORG_{v-stop}}$ and $\mathrm{CLR_{v-stop}}$), as the rocks could theoretically move with a very low velocity slightly above the stopping criterion (= 0.5 $\mathrm{m{\cdot}s^{-1}}$) for several seconds and distort the mean velocity value. However, this was not observed, as $\mathrm{ORG_{v-stop}} = 1.5 \pm 0.4$ and $\mathrm{CLR_{v-stop}} = 1.3 \pm 0.4 \mathrm{m{\cdot}s^{-1}}$ are distinctly higher than the stopping criterion. We conclude that the stopping process of the rocks is simulated close to reality. Consequently, we deduce that the translational velocity is slightly underestimated over longer distances. The accurate treatment of the entire deceleration phase of rocks represents a demanding challenge for any rockfall code, in particular in this low-weight class regime. In the given experimental set-up solely the runtimes determine the mean rock velocity and thus the translational kinetic energy, the most crucial output variable of rockfall simulation programs. Hence, four main limitations came to our attention during the study, which leads to new practically relevant follow-up research questions and hypotheses, and should be included in future experimental campaigns:

1. The investigated rock mass of 45 kg represents in many stratigraphic units a common rockfall release volume with a high occurrence probability and small return period. Nevertheless, with energies, $\leq$ 3 kJ only low rockfall intensities are achieved (FOEN, 2016). The verification of the rockfall stopping capacity under higher energies remains to be investigated.

2. The deposition pattern data in different forest conditions is unique and allowed to examine the performance of the presented three-dimensional deadwood, both experimentally and numerically. The available, additional in situ measurement data fostered an in-depth model calibration. However, the evaluations showed that (for example) a visual check of the impact location at high acceleration measurement values is desirable. Although challenging due to the visibility restrictions because of the trees (Bourrier et al., 2012), a slope-wide reconstruction of the rock velocities would complete the set of the parameters of interest (Caviezel et al., 2019a). A broader visual coverage enables the potential development of automated tree impact detection within the in situ sensor data.

3. Only compact rock shapes (Sneed and Folk, 1958) were used in this study. The results of open land experiments emphasize the importance of different rock shapes (Caviezel et al., 2021). Investigation on rockfall simulations in forests incorporating different rock shapes (Lu et al., 2020) show the importance of real-scale experiments as a calibration basis as different contact behavior and MROD are expected.

4. The fresh deadwood used here originates from trees felled on site. However, for forestry practice, it is also relevant to know how decomposed deadwood protects against rockfall, and how this effect is changing over time. It is essential to understand the potential adverse long-term effects of rocks deposited temporarily behind decaying deadwood as they may act as secondary rockfall sources.

Despite these still existing limitations and open questions, our results indicate that the complete removal of lying deadwood after natural disturbances or logging operations can lead to a substantial decrease in rockfall protection. While our experiments also allow us to quantify such effects, more experiments and long-term studies are needed to fully quantify them for different settings and to optimise their implementation in rockfall simulation models and management guidelines.

5 Conclusions

This experimental rockfall trilogy with 45 kg, cubic shaped rocks within different states of the forest, highlights the high protection capacity of partly piled deadwood against low-energy rockfalls. This is of general interest, as natural disturbances causing piled deadwood are suggested to increase in future. The ratio between the rock diameter and the overall deadwood height might have a decisive impact on the rock stopping capacity, whose thorough quantification needs further research. The agreement achieved between the simulations and the experiments is particularly convincing for the mean run-out distance, while it somewhat underestimates the lateral dispersion of the deposition points. The presented three-dimensional deadwood logs within the simulations performed realistically which affirms the demand for the inclusion of deadwood in rockfall simulations. This will allow forest managers to base their future dead wood management after natural disturbances, thinning, sanitary felling and regeneration gaps on a larger scientific basis. Based on our experimental results, we recommend at least in the case of relatively small expected rock sizes with low deadwood log breakage probability to consider supplementing the natural protection of the ecological infrastructure with additional transverse, lying deadwood logs as a cost-effective, economical, ecological, nature-based protection measure. Thanks to the extended model outcomes presented here, the benefits of these measures can be evaluated and thus planned in a more systematic manner, which in turn could reduce the overall economic costs. Future studies should focus on higher rockfall energies, where the rock velocities are completely retrievable, the influence of the rock shape is in-depth examined and long-term effects after partial decay of deadwood in post-disturbance stands are taken into account.

Data availability. The experimental deposition points, the in situ StoneNode data and the FI-detection $Matlab$ script as well as the input data for the rockfall simulation (DEM, tree file, release point and .rts files of the trees) are publicly available under doi:10.16904/envidat.248.

Author contributions. AR performed the data analysis, conceived the simulations and wrote the manuscript based on discussions and improvements from all authors, ES, AC, AR carried out the model calibration, AC conceived the experiment. AC, YB, KS, SD, AS carried out the experiments. KS, MK and DM conducted the forest inventory. YB and AS operated the GNSS and GL and MC programmed the deadwood Module.

Competing interests. The authors declare that they have no conflict of interest.

Acknowledgements. We thank the forest owner: the municipality of Albula/Alvra, Switzerland, and the AWN, Region 4, Tiefencastel for the permission to conduct experiments on the Surava site. The research was partially funded by the National Research Program "Sustainable Economy: resource-friendly, future-oriented, innovative" (NRP 73) by the Swiss National Science Foundation (Grant number: 407340_172415) and is part of the WSL research program Climate Change Impacts on Alpine Mass Movements (CCAMM).

References

Ammann, M.: Schutzwirkung abgestorbener Bäume gegen Naturgefahren, Eidg. Forschungsanstalt für Wald Schnee und Landschaft WSL, Birmensdorf, 2006.

Bourrier, F., Dorren, L. K. A., and Berger, F.: Full scale field tests on rockfall impacting trees felled transverse to the slope, in: Conference proceedings / 12th Congress Interpraevent, edited by Koboltschnig, G. and Huebl, J., pp. 643–650, International Research Society INTERPRAEVENT, Klagenfurt, 2012.

Caviezel, A., Schaffner, M., Cavigelli, L., Niklaus, P., Buhler, Y., Bartelt, P., Magno, M., and Benini, L.: Design and Evaluation of a Low-Power Sensor Device for Induced Rockfall Experiments, IEEE T INSTRUM MEAS, 67, 767–779, https://doi.org/10.1109/TIM.2017.2770799, 2018.

Caviezel, A., Demmel, S. E., Ringenbach, A., Bühler, Y., Lu, G., Christen, M., Dinneen, C. E., Eberhard, L. A., von Rickenbach, D., and Bartelt, P.: Reconstruction of four-dimensional rockfall trajectories using remote sensing and rock-based accelerometers and gyroscopes, EARTH SURF DYNAM, 7, 199–210, https://doi.org/10.5194/esurf-7-199-2019, 2019a.

Caviezel, A., Lu, G., Demmel, S. E., Ringenbach, A., Bühler, Y., Christen, M., and Bartelt, P.: RAMMS::ROCKFALL - a modern 3-dimensional simulation tool calibrated on real world data, in: 53rd US rock mechanics/geomechanics symposium, edited by American Rock Mechanics Association, vol. 19-223, 2019b.

Caviezel, A., Ringenbach, A., Demmel, S. E., Dinneen, C. E., Krebs, N., Bühler, Y., Christen, M., Meyrat, G., Stoffel, A., Hafner, E., Eberhard, L. A., von Rickenbach, D., Simmler, K., Mayer, P., Niklaus, P. S., Birchler, T., Aebi, T., Cavigelli, L., Schaffner, M., Rickli, S., Schnetzler, C., Magno, M., Benini, L., and Bartelt, P.: The relevance of rock shape over mass—implications for rockfall hazard assessments, NAT COMMUN, 12, 15, https://doi.org/10.1038/s41467-021-25794-y, 2021.

Costa, M., Marchi, N., Bettella, F., Bolzon, P., Berger, F., and Lingua, E.: Biological Legacies and Rockfall: The Protective Effect of a Windthrown Forest, Forests, 12, 1141, https://doi.org/10.3390/f12091141, 2021.

Dorren, L. K.: Rockyfor3D: Description of the complete 3D rockfall model, 2012.

Dorren, L. K. A.: FINT – Find individual trees: User manual, 2017.

Dorren, L. K. A. and Berger, F.: Stem breakage of trees and energy dissipation during rockfall impacts, TREE PHYSIOL, 26, 63–71, https://doi.org/10.1093/treephys/26.1.63, 2005.

Dupire, S., Bourrier, F., Monnet, J.-M., Bigot, S., Borgniet, L., Berger, F., and Curt, T.: Novel quantitative indicators to characterize the protective effect of mountain forests against rockfall, ECOL INDIC, 67, 98–107, https://doi.org/10.1016/j.ecolind.2016.02.023, 2016.

ETAG 027: Guidline for European Technical Approval of Falling Rock Protection Kits, last checked 27.02.18., https://www.eota.eu/en-GB/content/etags-used-as-ead/26/, 2013.

Feser, F., Barcikowska, M., Krueger, O., Schenk, F., Weisse, R., and Xia, L.: Storminess over the North Atlantic and northwestern Europe-A review, Q J ROY METEOR SOC, 141, 350–382, https://doi.org/10.1002/qj.2364, 2015.

FOEN: Protection against Mass Movement Hazards: Guideline for the integrated hazard management of landslides, rockfall and hillslope debris flows, https://www.bafu.admin.ch/dam/bafu/en/dokumente/naturgefahren/uv-umwelt-vollzug/schutz_vor_massenbewegungsgefahren.pdf.download.pdf/protection_againstmassmovementhazards.pdf, 2016.

Fuhr, M., Bourrier, F., and Cordonnier, T.: Protection against rockfall along a maturity gradient in mountain forests, FOREST ECOL MANAG, 354, 224–231, https://doi.org/10.1016/j.foreco.2015.06.012, 2015.

Isenburg, M.: LAStools, https://rapidlasso.com/lastools/, 2021.

Jain, P., Tye, M. R., Paimazumder, D., and Flannigan, M.: Downscaling fire weather extremes from historical and projected climate models, CLIMATIC CHANGE, 163, 189–216, https://doi.org/10.1007/s10584-020-02865-5, 2020.

Jönsson, A. M., APPELBERG, G., HARDING, S., and BÄRRING, L.: Spatio-temporal impact of climate change on the activity and voltinism of the spruce bark beetle, Ips typographus, GLOB CHANGE BIOL, 15, 486–499, https://doi.org/10.1111/j.1365-2486.2008.01742.x, 2009.

Killick, R., Fearnhead, P., and Eckley, I. A.: Optimal detection of changepoints with a linear computational cost, J AM STAT ASSOC, 107, 1590–1598, https://doi.org/10.1080/01621459.2012.737745, 2012.

Kulakowski, D., Seidl, R., Holeksa, J., Kuuluvainen, T., Nagel, T. A., Panayotov, M., Svoboda, M., Thorn, S., Vacchiano, G., Whitlock, C., Wohlgemuth, T., and Bebi, P.: A walk on the wild side: Disturbance dynamics and the conservation and management of European mountain forest ecosystems, FOREST ECOL MANAG, 388, 120–131, https://doi.org/10.1016/j.foreco.2016.07.037, 2017.

Lanfranconi, C., Sala, G., Frattini, P., Crosta, G. B., and Valagussa, A.: Assessing the rockfall protection efficiency of forests at the regional scale, LANDSLIDES, 17, 2703–2721, https://doi.org/10.1007/s10346-020-01458-8, 2020.

Lu, G., Caviezel, A., Christen, M., Demmel, S. E., Ringenbach, A., Bühler, Y., Dinneen, C. E., Gerber, W., and Bartelt, P.: Modelling rockfall impact with scarring in compactable soils, LANDSLIDES, 64, 41, https://doi.org/10.1007/s10346-019-01238-z, 2019.

Lu, G., Ringenbach, A., Caviezel, A., Sanchez, M., Christen, M., and Bartelt, P.: Mitigation effects of trees on rockfall hazards: does rock shape matter?, LANDSLIDES, 50, 1689, https://doi.org/10.1007/s10346-020-01418-2, 2020.

Lundström, T., Jonsson, M. J., Volkwein, A., and Stoffel, M.: Reactions and energy absorption of trees subject to rockfall: a detailed assessment using a new experimental method, TREE PHYSIOL, 29, 345–359, https://doi.org/10.1093/treephys/tpn030, 2009.

Moos, C., Dorren, L. K. A., and Stoffel, M.: Quantifying the effect of forests on frequency and intensity of rockfalls, NAT HAZARD EARTH SYS, 17, 291–304, https://doi.org/10.5194/nhess-17-291-2017, 2017.

Mozny, M., Trnka, M., and Brázdil, R.: Climate change driven changes of vegetation fires in the Czech Republic, THEOR APPL CLIMATOL, 143, 691–699, https://doi.org/10.1007/s00704-020-03443-6, 2021.

Niklaus, P., Birchler, T., Aebi, T., Schaffner, M., Cavigelli, L., Caviezel, A., Magno, M., and Benini, L.: StoneNode: A low-power sensor device for induced rockfall experiments, in: 2017 IEEE Sensors Applications Symposium (SAS), pp. 1–6, IEEE, https://doi.org/10.1109/SAS.2017.7894081, 2017.

Olmedo, I.: Felled trees as rockfall protection devices: Experimental and numerical studies, Doctoral thesis, irstea, Lyon, https://doi.org/10.13140/RG.2.1.2179.8640, 2015.

Olmedo, I., Bourrier, F., Bertrand, D., Toe, D., Berger, F., and Limam, A.: Experimental analysis of the response of fresh wood stems subjected to localized impact loading, WOOD SCI TECHNOL, 49, 623–646, https://doi.org/10.1007/s00226-015-0713-0, 2015.

Olmedo, I., Bourrier, F., Bertrand, D., Berger, F., and Limam, A.: Dynamic analysis of wooden rockfall protection structures subjected to impact loading using a discrete element model, European Journal of Environmental and Civil Engineering, 24, 1430–1449, https://doi.org/10.1080/19648189.2018.1472042, 2020.

Rammer, W., Brauner, M., Dorren, L. K. A., Berger, F., and Lexer, M. J.: Evaluation of a 3-D rockfall module within a forest patch model, NAT HAZARD EARTH SYS, 10, 699–711, https://doi.org/10.5194/nhess-10-699-2010, 2010.

Schelp, C.: plot_confidence_ellipse.py: A function to plot the confidence ellipse of the covariance of a 2D dataset. Uses matplotlib., https://gist.github.com/CarstenSchelp/b992645537660bda692f218b562d0712, 2018.

Sneed, E. D. and Folk, R. L.: Pebbles in the lower Colorado River, Texas, study in particle morfogenesis, J GEOL, 66, 114–150, 1958.

Sommerfeld, A., Rammer, W., Heurich, M., Hilmers, T., Müller, J., and Seidl, R.: Do bark beetle outbreaks amplify or dampen future bark beetle disturbances in Central Europe?, J ECOL, 109, 737–749, https://doi.org/10.1111/1365-2745.13502, 2021.

Stoffel, M., Wehrli, A., Kühne, R., Dorren, L. K. A., Perret, S., and Kienholz, H.: Assessing the protective effect of mountain forests against rockfall using a 3D simulation model, FOREST ECOL MANAG, 225, 113–122, https://doi.org/10.1016/j.foreco.2005.12.030, 2006.

Toe, D., Bourrier, F., Olmedo, I., Monnet, J.-M., and Berger, F.: Analysis of the effect of trees on block propagation using a DEM model: implications for rockfall modelling, LANDSLIDES, 14, 1603–1614, https://doi.org/10.1007/s10346-017-0799-6, 2017.

Woltjer, M., Rammer, W., Brauner, M., Seidl, R., Mohren, G. M. J., and Lexer, M. J.: Coupling a 3D patch model and a rockfall module to assess rockfall protection in mountain forests, J ENVIRON MANAGE, 87, 373–388, https://doi.org/10.1016/j.jenvman.2007.01.031, 2008.

Wunder, J., Knüsel, S., Dorren, L., Schwarz, M., Bourrier, F., and Conedera, M.: Götterbaum und Paulownie: die «neuen Wilden» im Schweizer Wald?, Schweizerische Zeitschrift für Forstwesen, 169, 69–76, https://doi.org/10.3188/szf.2018.0069, 2018.